Cerebral Cortex November 2006;16:1584-1594
doi:10.1093/cercor/bhj095
Advance Access publication December 28, 2005

Cross-sectional and Longitudinal Analyses of Anatomical Sulcal Changes Associated with Aging

Maryam E. Rettmann[1,2], Michael A. Kraut[3], Jerry L. Prince[4] and Susan M. Resnick[1]

[1]National Institute on Aging, National Institutes of Health, Baltimore, MD 21224, USA, [2]Department of Biomedical Engineering, Johns Hopkins University, Baltimore, MD 21205, USA, [3]Department of Radiology, Johns Hopkins University, Baltimore, MD 21287, USA and [4]Department of Electrical and Computer Engineering, Johns Hopkins University, Baltimore, MD 21218, USA

Imaging studies of the human brain indicate that the cortex undergoes anatomic changes during the aging process. With the ability to study the human brain in vivo using magnetic resonance imaging, understanding the nature and location of these changes is of increasing interest. In this work, we investigate cross-sectional and longitudinal age effects on the geometric shape and gray matter (GM) volume for regions of interest on the cortical surface. Each of the regions corresponds to the buried cortex surrounding the sulcal spaces and is termed a "sulcal region." The study consists of 35 older adults scanned three times over a 4-year time span. The group includes 19 women and 16 men ranging in ages from 59 to 84 years (mean 70.9, standard deviation 6.2). We analyze 8 sulcal regions—the buried cortex surrounding the left and right central, superior frontal, cingulate, and parietooccipital sulci. We examine surface area, GM thickness, GM volume, sulcal depth, local gyrification index, and measures of curvature. Results indicate cross-sectional age effects in mean thickness, GM volume, sulcal depth, and curvature characteristics of sulcal regions. In addition, we found longitudinal decreases in surface area, mean thickness, GM volume, and sulcal depth measures as well as changes in sulcal curvature.

Keywords: aging, brain, cortex, cortical atrophy, cortical shape changes, sulci

Introduction

With the advent and rapid development of magnetic resonance imaging (MRI) techniques, it is now possible to conduct in vivo studies of the effects of aging on the human brain. Analysis of magnetic resonance (MR) images, including sophisticated image processing techniques as well as cortical surface reconstruction algorithms, provides the ability to analyze both cortical atrophy and anatomical shape changes associated with aging. Cortical changes have been quantified using both global and regional analyses. Whereas global analyses give an overall indication of change associated with aging, regional studies allow for the localized investigation of age changes in regions that may correspond to specific functions. Age effects can also be assessed in either a cross-sectional or longitudinal fashion. Cross-sectional imaging studies provide insights into age differences in cortical anatomy; however, longitudinal studies are required to provide a true measure of cortical change over time.

Cross-sectional analyses assessing global differences have indicated smaller gray, white, and total brain volumes (Jernigan and others 1990; Gur and others 1991; Pfefferbaum and others 1994; Mueller and others 1998; Courchesne and others 2000; Resnick and others 2000; Good and others 2001; Liu and others 2003; Scahill and others 2003; Sullivan and others 2004) in older versus younger individuals. In a study including subjects from a broad age range, thinner cortices in older versus younger individuals were reported, as well as differences in the global morphological shape of the cortical surface (Magnotta and others 1999).

A variety of approaches has been described in the literature for regional analyses of cross-sectional cortical age differences. One of the main challenges in region-based approaches is the definition and reliable identification of cortical regions of interest (ROIs) from the MR images. Several groups have defined ROIs on the cortex using anatomical landmarks and boundaries followed by the manual tracing of these regions. In 1 study, 11 cortical regions were manually traced on MR image cross-sections with the largest differences observed in the prefrontal gray matter (GM) (Raz and others 1997). Other studies using manual tracing (often in conjunction with "computer-assisted" techniques) have found age-related volume differences in frontal (Coffey and others 1992; Cowell and others 1994; DeCarli and others 1994; Mueller and others 1998; Tisserand and others 2002), temporal (Coffey and others 1992; Sullivan and others 1995; Mueller and others 1998; Scahill and others 2003), and parietal–occipital (Murphy and others 1996) regions with smaller volumes in the older versus younger individuals. One advantage of manual tracing is that it allows for the consideration of individual anatomical differences and therefore a presumably more accurate definition of cortical structures. Disadvantages, however, are that manual tracing is time consuming and sometimes unreliable, and therefore, the number of studies and regions examined are restricted.

Automated approaches are appealing in that they can be applied to a large number of subjects, and they eliminate the variability inherent in manual interaction. Popular automated approaches for regional-based cortical analysis include defining ROIs in a standardized space, voxel-based morphometry (VBM) (Ashburner and Friston 2000), and average map techniques. In a study of older adults (Resnick and others 2000), brain lobes were automatically defined in a standardized space, and the parietal lobe was shown to exhibit the largest age effects. In a VBM study of subjects over a broad age range (Good and others 2001), larger GM declines were shown to occur in the insula, superior parietal gyri, central sulci, and cingulate sulci. One study (Tisserand and others 2002) utilized each of the aforementioned methodologies—that is, manual tracing, transformation into a standardized space, and VBM for dividing the frontal lobe into various ROIs. They concluded that subregions of the frontal lobe do change differentially with age, but the regions found to undergo more or less change were dependent on the method used. "Average map" approaches include aligning cortical surface models from multiple subjects and displaying results on a single representation of the cortical

surface. This type of approach has been utilized to demonstrate regionally dependent age differences in GM density (Sowell and others 2003) and cortical thickness (Salat and others 2004). The optimal approach for regional cortical analysis remains unclear, but it is possible that each yields complimentary information.

Longitudinal analyses have also demonstrated cortical atrophy with age. One analysis of older adults, spanning a 4-year interval (Resnick and others 2003), reported decreases in cortical GM. This study also demonstrated differential tissue loss across lobes (frontal and parietal greater than temporal and occipital), as well as vulnerability of local brain regions through voxel-based analysis. In a longitudinal analysis over 3–6 years (Mueller and others 1998), in which healthy, elderly subjects were divided into 3 different age groups, volumetric differences were found between the groups; however, there were no significant differences in the rates of changes between the 3 groups. Another longitudinal study of older individuals (Tang and others 2001), which utilized stereological techniques, reported a decline in total cerebral volume. A recent study of subjects over a broad age range (Scahill and others 2003) also reported longitudinal atrophy for the whole brain as well as the temporal lobes. Another recent study (Liu and others 2003) assessed subjects in 3 age groups and reported significant declines in total brain volume in both the middle and older groups.

Evidence from the literature therefore suggests that the brain undergoes anatomical changes during the aging process, and these changes appear to occur differentially across various brain regions. However, the nature of these region-specific changes remains unclear. In this work, we use cortical geometry to quantify anatomical changes in specific cortical regions and investigate both shape changes and GM atrophy. Our cortical ROIs are defined using the cortical sulci and are termed "sulcal regions" (Rettmann and others 2002). More specifically, they are defined as the buried cortex surrounding the sulcal spaces. Our approach is analogous to a manual tracing approach in that we define ROIs on each subject taking individual variability into account. However, in our approach, each buried cortical region is segmented using an automated algorithm (Rettmann and others 2002). A user can then identify specific sulcal ROIs (i.e., central, superior frontal, etc.) by clicking on the automatically segmented regions (Rettmann and others 2005). Our approach is advantageous in that it accounts for individual variability; yet it includes a significant automated component and is therefore less time consuming and more reliable than a purely manual approach. We specifically chose to study sulcal regions as opposed to gyral regions because boundaries for the sulcal regions can be defined more consistently than for the gyral regions. This allows for a robust and repeatable segmentation of the sulcal regions (Rettmann and others 2005), which is essential in the context of an aging study.

The framework of this approach is similar in spirit to that of Mangin and others (2004) in which the structures of interest are also the cortical sulci. Using surfaces to represent the sulcal spaces, along with maps of the cerebrospinal fluid (CSF) within the sulci, older individuals were shown to have wider sulci with a larger fraction of CSF than younger individuals (Kochunov and others 2005). The most pronounced differences were found in the cingulate, frontal, and parietal lobes.

In this work, we are interested in assessing age-related changes in cortical sulcal geometry. For each sulcal ROI, we define and compute a collection of features (e.g., surface area, volume, depth, thickness, and curvature) and use these values to quantify anatomic sulcal structure. These features are then analyzed, both cross-sectionally and longitudinally, in 35 subjects (19 women, 16 men, age range 59–84, mean 70.9, standard deviation 6.2). The longitudinal analysis includes data at 3 time points across a 4-year interval. Our findings suggest that there are age changes in geometric shape as well as cortical atrophy for specific sulcal regions.

Materials and Methods

Subjects

All MR imaging data used in this work were obtained from the neuroimaging study of the Baltimore longitudinal study of aging (BLSA) (Shock and others 1984; Resnick and others 2000). All subjects were scanned with a GE Signa 1.5-T scanner (GE Healthcare, Waukesha, WI) using a T_1-weighted SPGR imaging protocol (TR = 35 ms, TE = 5 ms, flip angle = 45°, NEX = 1, voxel dimensions of 0.94 × 0.94 × 1.5–mm slice thickness). A total of 35 individuals were analyzed at 3 time points—baseline (year 1), year 3, and year 5. Participants in this sample are a subset of BLSA volunteers, aged 59–85 at baseline, who agreed to return annually and who did not meet any of the following exclusionary criteria at initial evaluation: central nervous system disease (epilepsy, stroke, bipolar illness, prior diagnosis of dementia according to diagnostic and statistical manual-III-R criteria [Spitzer and Williams 1987]), severe cardiovascular disease (myocardial infarction, coronary artery disease requiring angioplasty, or bypass surgery), severe pulmonary disease, or metastatic cancer. All participants remained free of dementia at year 5 follow-up, using diagnostic procedures described previously (Kawas and others 2000). This research protocol was approved by the local Institutional Review Board, and written informed consent was obtained from all participants in conjunction with each neuroimaging visit. All participants in the sample used for this study were right handed. Other demographic details of this group are given in Table 1.

Image Analysis

We use the basic approach that has been previously described in Xu and others (1999) to find a cortical surface lying at the geometric center of the cortex from a volumetric MR image. We chose to represent the cortex as a surface lying at the geometric center of the GM as we believe this best represents the cortical geometry. Techniques reported in Xu and others (2000), Han, Xu, and others (2001), and Han and others (2002, 2003) were used to improve upon the original methodology. Cortical reconstruction using implicit surface evolution (CRUISE) is the current set of algorithms comprising this basic approach with the improvements as described in Han, Xu, and Prince (2001) and Han and others (2004).

The first step in the CRUISE processing stream is to remove the cerebellum, extracranial tissue, and brain stem using a semiautomated approach (Goldszal and others 1998). Second, a fuzzy segmentation algorithm, that is robust to both noise and tissue inhomogeneities (Pham and Prince 1999; Pham 2001), is applied to this MR image volume yielding 3 membership function image volumes representing

Table 1
Participant demographics at baseline

	Men	Women	Combined
N	16	19	35
Age (years), range	72.3 (6.1), 63.4–84.4	69.8 (6.2), 59.6–81.1	70.9 (6.2), 59.6–84.4
Education (years)	16.4 (3.0)	16.4 (2.4)	16.4 (2.7)
MMS	28.7 (1.4)	28.8 (1.1)	28.8 (1.3)
BMS	0.6 (0.7)	0.9 (1.5)	0.8 (1.2)

Note: MMS, mini-mental state examination; BMS, blessed information memory concentration test. The baseline MMS scores were missing for 2 subjects, and the baseline BMS score was missing for 1 subject. For these cases, the closest available scores (typically within 1 year) were substituted.

the fractions of white matter (WM), GM, and CSF within each image volume. The third step is to automatically fill the ventricles and subcortical GM structures (e.g., putamen, thalamus) within the WM membership function (Han, Xu, and others 2001). Fourth, a triangulated surface mesh, lying at the GM–WM interface, is generated, which serves as an initial surface for finding the final, central surface. The GM–WM interface can be approximated by computing the 0.5 isolevel of the WM membership function. Because of noise and partial volume averaging, an isosurface generated from the processed WM membership function typically contains hundreds of handles (like that on a coffee cup). In order to remove the handles from the WM membership function volume before its isosurface is computed, we use a graph-based topology correction algorithm (Han and others 2002). In addition, partial volume effects within the GM can make adjacent GM banks within narrow sulci barely distinguishable. To compensate for this, CRUISE uses anatomically consistent enhancement (ACE) (Xu and others 2000; Han, Xu, and Prince 2001), which automatically edits the GM membership function, creating thin (artificial) CSF separations within sulci. Finally, a topology-preserving geometric deformable surface model (Han and others 2003), initialized at the GM/WM surface, is driven toward the geometric center of the GM using forces derived from the ACE-edited GM membership function. A typical result of a cortical surface generated with the CRUISE algorithms is shown in Figure 1.

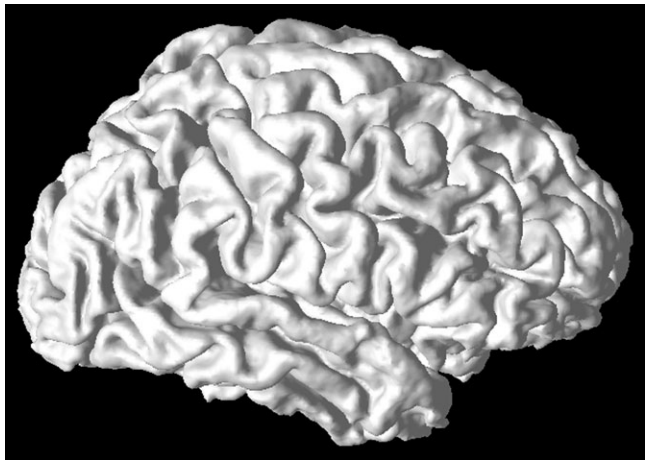

Figure 1. A typical result of the cortical surface reconstruction procedure.

After obtaining the cortical surface, the next step is to segment the ROIs—that is, the sulcal regions. Each sulcus has a corresponding sulcal region, defined as the portion of the cortical surface surrounding the space of the sulcus, as illustrated on a cross-section of a cortical surface in Figure 2. We use a previously described watershed segmentation algorithm (Rettmann and others 2002) to segment the sulcal regions from the cortical surface. A brief overview of this technique follows. First, the hemispheres are separated so the medial sulcal regions are also segmented. Next, the geodesic depth is computed for each vertex on the triangle mesh that lies within a sulcal region using the fast marching technique (Kimmel and Sethian 1998). The geodesic depth is defined as the length of the shortest path, along the surface, from each point within a sulcal region to the "outer cortex" where we define outer cortex as the part of the cortex that is visible without opening up the cortical folds. The outer cortex is found using a shrink-wrap deformable surface where the forces are defined such that the shrink-wrap surface tightly surrounds the cortical surface but does not enter into the cortical folds. All points on the cortical surface that are less than 2 mm from the shrink-wrap surface are defined as outer cortex, other points are defined as buried cortex. A watershed transform (cf., Meyer and Beucher 1990; Vincent and Soille 1991) is then computed on the triangle mesh using a "height function" defined as the maximum geodesic depth minus the actual geodesic depth. The watershed algorithm segments a distinct region called a catchment basin for each local minimum of the height function; however, a typical problem with the watershed algorithm is that of oversegmentation. In our case, this results in several catchment basins representing a single sulcal region. The oversegmentation is addressed by utilizing an algorithm that merges appropriate catchment basins.

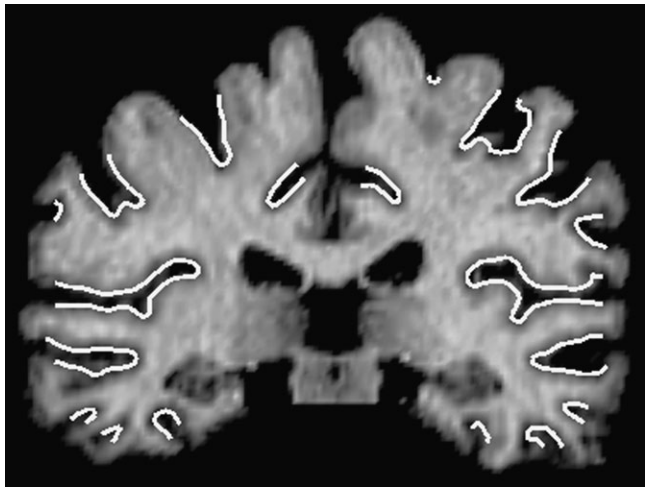

Figure 2. Cross-section of cortical surface illustrating sulcal regions. Sulcal regions are outlined in white.

The result of applying the sulcal segmentation algorithm to the surface in Figure 1 is shown in Figure 3*a*. Each sulcal region is itself a 3-dimensional triangulated surface. Examples of the left and right central sulcal regions are shown in Figure 3*b,c*. Each of these segmented regions must subsequently be assigned a corresponding neuroanatomical label. We label each sulcal region according to its associated sulcus—that is, the buried cortical region surrounding the central sulcus is called the central sulcal region. At present, a user must manually assign these anatomical labels to each of the automatically segmented regions. This is accomplished in an efficient fashion with the assistance of a user interface called the Program for Assisted Labeling of Sulcal Regions (PALS)—a detailed description of this procedure along with its validation can be found in Rettmann and others (2005).

There were 2 main goals for the labeling procedure. The first was to accurately label each of the sulcal regions according to anatomic convention. We followed the convention outlined in Ono's Atlas of the cerebral sulci (Ono and others 1990) for defining sulcal patterns, interruptions, and the location of junctions between connected sulci. We analyzed 4 sulcal regions on each cortical hemisphere—the left and right central, left and right superior frontal, left and right cingulate, and left and right parietooccipital regions. The locations of these sulcal regions are shown in Figure 4. For the central sulcus, if it extended into the Sylvian fissure, the end of the sulcus was defined at the boundary between the central and Sylvian. In addition, any connections with the precentral or postcentral sulci were removed. The cingulate sulcus can be either continuous or interrupted to 2 or 3 segments. If interrupted, all pieces were included in the analysis. In addition, the marginal ramus (i.e., the posterior end) of the cingulate was included. Connections with the subparietal and superior rostral sulci were removed. In the case of a double parallel pattern, both the superior and inferior segments of the sulcus were included. The superior frontal sulcus can be continuous or interrupted to 2, 3, or 4 segments. If interrupted, all pieces were included. In addition, connections with the precentral, frontomarginal, and intermediate frontal were removed. For the parietooccipital sulcal region, connections to the calcarine and sagittal sulcus of the cuneus were removed.

The second goal in the labeling procedure was to consistently label the sulcal regions across the 3 scans for each individual. This is important for the longitudinal analysis because it is critical that the sulcal regions are labeled exactly the same across the multiple scans in order to ensure that even small cortical changes can be detected. For example, changes in GM volume could potentially be in the order of the

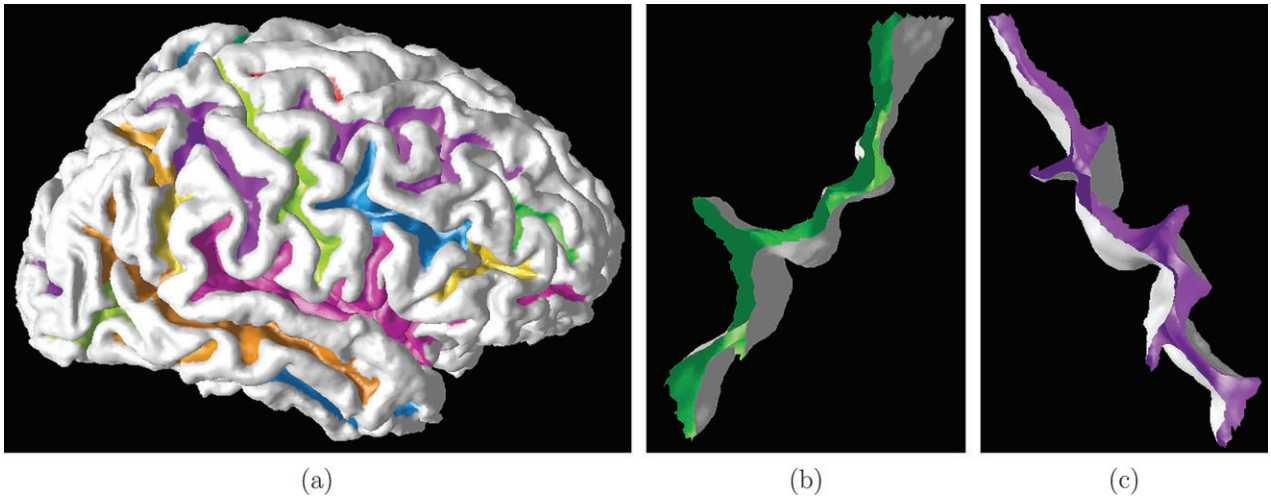

Figure 3. (*a*) The sulcal segmentation corresponding to Figure 1. (*b*) Left and (*c*) right central sulcal regions.

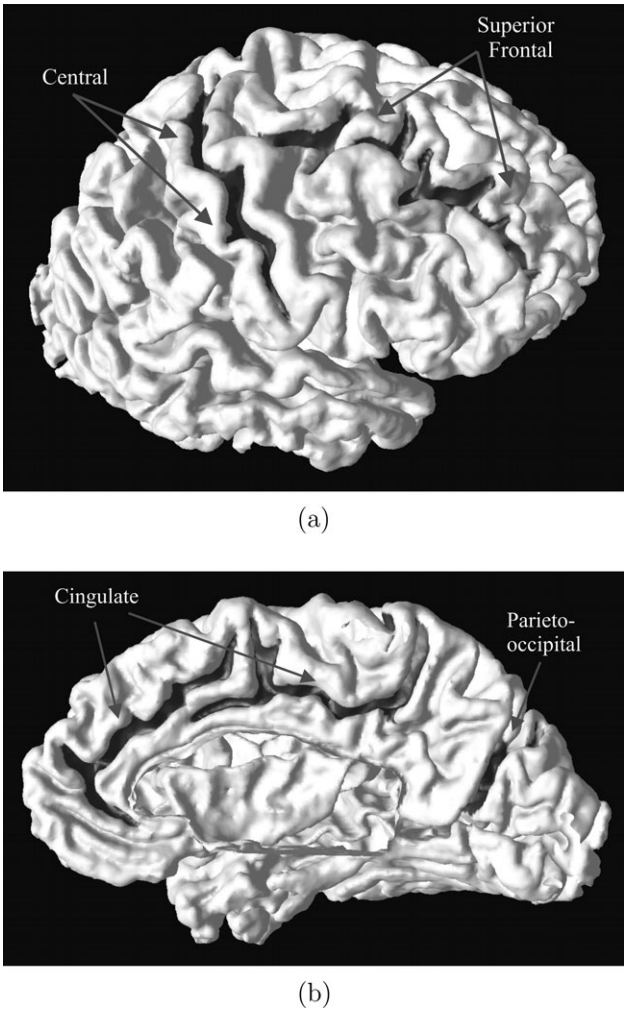

Figure 4. The locations of the sulcal regions labeled on (*a*) the lateral surface and (*b*) the medial surface.

size of a small side branch of a sulcus. Therefore, in the labeling procedure, we had to ensure that a sulcal side branch was consistently either included or excluded across all 3 scans. For this reason, the rater labeled the 3 scans corresponding to a single subject in parallel but remained blinded to age, year of scan, and other demographic characteristics. After labeling the sulcal region for each time point, the rater could view and rotate the 3-dimensional segmented surfaces corresponding to each sulcal region. This provided a final check that the labeling had been done in a consistent fashion. A more detailed description of both the labeling interface and the labeling procedure can be found in Rettmann and others (2005). In addition, quantitative reliability experiments have been performed indicating both short-term repeatability and long-term stability of these techniques (Rettmann and others 2005).

The combination of these tools provides 3-dimensional surface representations of specific sulcal ROIs on the cortical surface. These regions can subsequently be analyzed according to their geometric properties. We next describe a collection of geometric features computed on the segmented and labeled sulcal regions, which provide quantitative information on the geometry of specific cortical ROIs. They include measures of surface area, GM thickness, GM volume, sulcal depth, gyrification index, and curvature. For each of these geometric features, we describe the measurement made and the technique used for its computation.

Surface Area

This measure quantifies the cortical surface area of a sulcal region, and its computation is described in Rettmann and others (2005). Essentially, area is computed as the sum of the areas of the triangles that lie within a sulcal region.

Thickness

We use the method described in Han, Xu, and Prince (2001) to compute cortical thickness. In this approach, cortical thickness is computed from the image volume using distance transforms from the GM–WM and GM–CSF interfaces. A thickness value is assigned to each grid point in the volume that lies between the 2 interfaces and is defined as the sum of the distances from the point to each of the 2 interfaces. The reconstructed cortical surface is generated in the same coordinate space as the image volume, which means that each vertex can obtain image values by directly mapping into the image data in the volume. Accordingly, we obtain measures of cortical thickness at each vertex using trilinear interpolation applied in the image volume containing estimates of cortical thickness at volumetric grid points.

GM Volume

The GM volume is a measure of the amount of cortical GM corresponding to each sulcal region, and its computation is described in Rettmann and others (2005). Essentially, volume is computed as the sum of the volumes of the individual triangles that lie within the labeled region, where the volume of each triangle is computed as the product of its area and the thickness at the center of the triangle.

Geodesic Depth

A description of this measure and its computation were previously reported in Rettmann and others (2002). The geodesic depth is defined as the length of the shortest path, along the surface, from each point within a sulcal region to the outer cortex. The outer cortex is defined as the part of the cortex that is visible without opening up the cortical folds. We use geodesic distance rather than 3-dimensional Euclidean distance as a measure of depth because it is a natural measure on the surface itself. For each sulcal region, we compute its mean geodesic depth by averaging all depth values in a sulcal region.

Local Gyrification Index

Gyrification index is a metric that quantifies the amount of cortex buried within the sulcal folds as compared with the amount of cortex on the "outer" visible cortex. It is typically computed by drawing 2 contours on cross-sectional slices of a brain (Zilles and others 1988) where 1 contour follows the outer cortical surface (i.e., that part of the cortex visible without opening up the cortical folds) and the other follows the entire cortical surface, including the buried cortex. The gyrification index is then defined as (length of complete contour)/(length of outer contour). Thus, a cortex with extensive folding has a large gyrification index, whereas a cortex with limited folding has a small gyrification index. In the extreme case, consider a cortex with no sulcal folds. The length of the complete and outer contours would be the same yielding a gyrification index of 1. As the number and size of sulcal folds increase, the length of the complete contour increases yielding a higher gyrification index. We propose a variation of this measure called the "local gyrification index." Although still quantifying cortical gyrification, this measure differs in that it indicates the local gyrification in regions associated with cortical sulci. In addition, our measure is a full 3-dimensional surface measurement as opposed to using contours on 2-dimensional cross-sections.

As described in Rettmann and others (2002), the sulcal segmentation technique can be extended within the same framework to compute a complete parcellation of the cortical surface where each parcellated unit is associated with a sulcal region. This is illustrated in Figure 5 where a typical sulcal segmentation is illustrated in 5*a* with the corresponding complete parcellation shown in 5*b*. Essentially, this parcellation is a technique for associating each point on the "gyral regions" to a sulcal region. In the definition of local gyrification index, the gyral regions are defined as the cortex that is not buried within the cortical folds (i.e., all cortex that is not part of the sulcal regions). The parcellation is accomplished by computing the geodesic distance transform from each sulcal region to the gyral regions. Each point on the gyral regions is subsequently associated with the sulcal region to which it has the minimum distance. The regional gyrification index for a particular sulcus is then computed as (area of the entire parcellated region)/(area of the gyral part of parcellated region only). Consider 2 parcellated regions with the same gyral area. The parcellated region with the larger sulcal fold will have a higher gyrification index.

Curvature

The mean curvature at a point on a surface can be used as a measure of how convex or concave the surface is at that point. The mean curvature is computed by averaging the maximum and minimum principle curvatures from a surface patch fitted around each vertex (Tao 2005). In this work, a convex point has positive mean curvature, and a concave point has negative mean curvature. To illustrate the curvatures within a sulcal region, the mean curvatures are displayed on a 3-dimensional rendering of the central sulcal region in Figure 6*a*. The color map goes from blue to red where shades of blue represent negative mean curvatures and shades of yellow, orange, and red represent positive mean curvatures.

We are interested in quantifying the percentage of points in a sulcal region lying on tight outward and inward bends of the cortical surface. This is accomplished by computing the percentage of high positive and high negative mean curvature points in each of the sulcal regions. We have measured 3 features associated with curvature for each sulcal region. The first measure is the percentage of high positive mean curvature points defined as the ratio of the number of vertices with a mean curvature above 0.1 and the total number of vertices in the sulcal region. This quantifies the percentage of points in the sulcal region lying on tight outward bends of the cortex as illustrated in Figure 6*b*. In this figure, all vertices with a mean curvature above 0.1 are colored in red, and the remaining vertices are colored white. For the percentage of high negative mean curvature points, we compute 2 measures. The first is the percentage of high negative curvature points defined as the ratio of the number of vertices with a mean curvature below –0.1 and the total number of vertices in the sulcal region. The second is the percentage of very high negative curvature points defined as the ratio of the number of vertices with a mean curvature below –0.3 and the total number of vertices in the sulcal region. These measures are illustrated in Figure 6*c*,*d*, respectively, where the vertices below the specified threshold are colored in blue and the remaining vertices are colored white. From this figure, we see that high negative curvature points lie on tight inward bends of the cortex, whereas very high negative curvature points tend to lie along the sulcal fundus.

In order to quantify how the choice of threshold affects the curvature metric, we conducted the following analysis. For each sulcal region, we computed the percentage of points above and below specified positive and negative thresholds. The threshold was varied from 0.01 to 0.40 at increments of 0.01 for the positive curvature analysis and from –0.40 to –0.01 at increments of 0.01 for the negative curvature analysis. The curvature metric varied smoothly with changes in the threshold value for all sulcal regions. Plots for the left central sulcal region are shown in Figure 7*a*,*b*. This figure illustrates that small changes in the threshold value will not result in abrupt changes in the curvature metric.

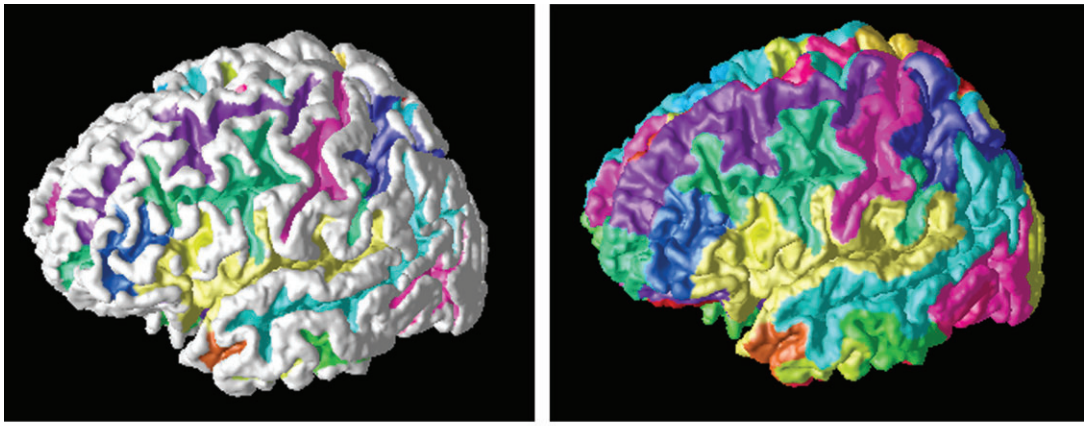

Figure 5. (*a*) A typical sulcal segmentation and (*b*) its corresponding cortical parcellation.

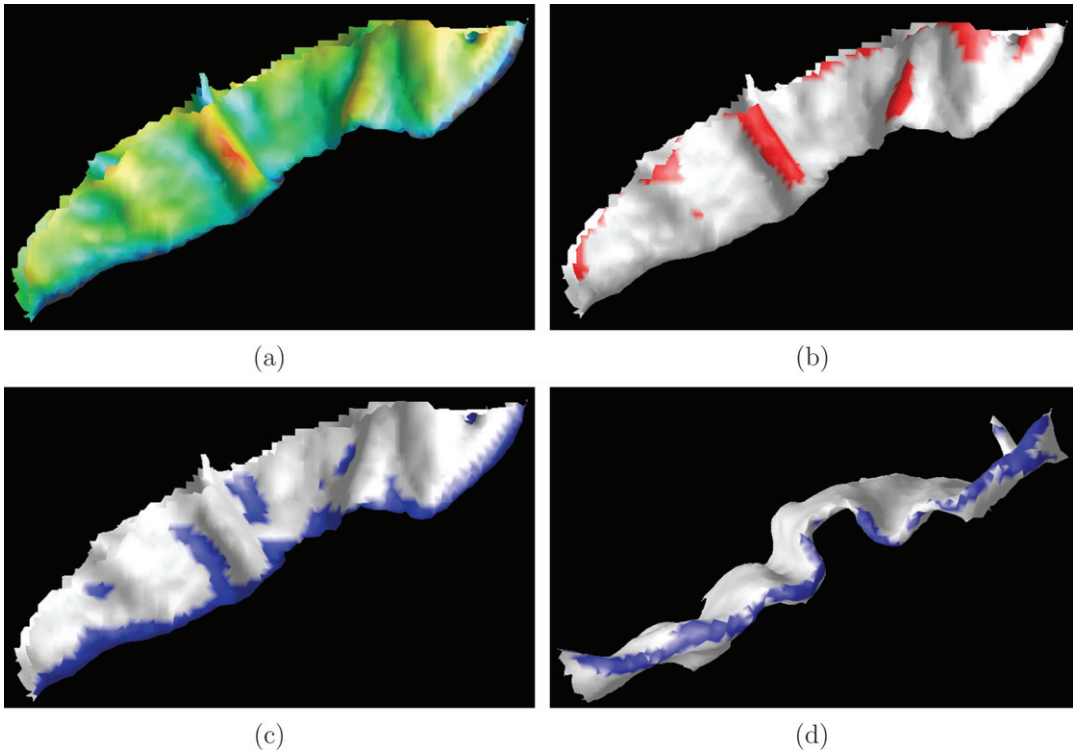

Figure 6. Central sulcal region displayed with the following: (*a*) mean curvature, (*b*) high positive curvature points (all vertices with mean curvature above 0.1 are colored red), (*c*) high negative curvature points (all vertices with mean curvature below –0.1 are colored blue), and (*d*) very high negative curvature points (all vertices with mean curvature below –0.3 are colored blue).

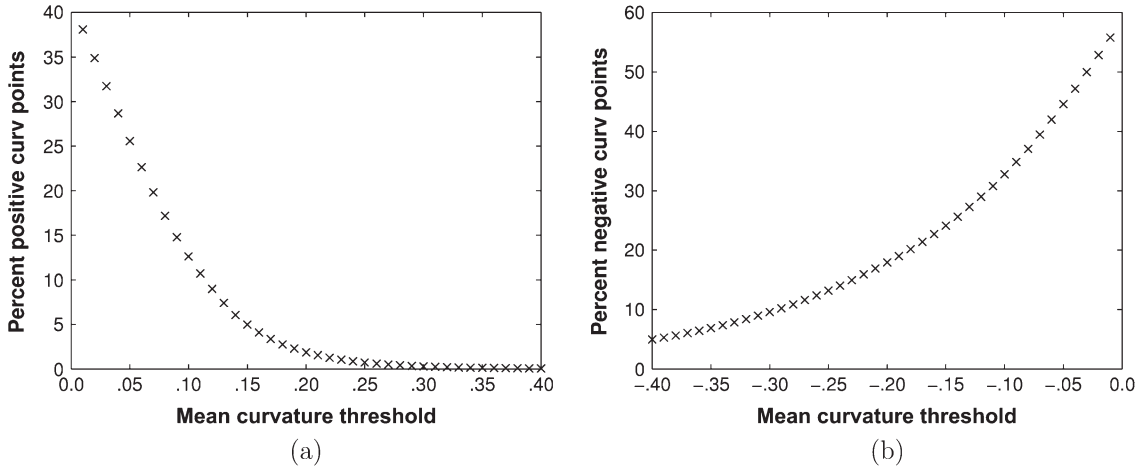

Figure 7. (*a*) Percentage of positive curvature points versus threshold and (*b*) percentage of negative curvature points versus threshold for the left central sulcal region.

Intracranial Volume

Intracranial volumes (ICVs) were computed for each subject to correct for individual differences in overall brain size in the statistical analysis. ICV is defined as the total volume of GM, WM, and CSF. ICVs were computed using the year 1 MRI for each individual with a HAMMER-based registration algorithm (Shen and Davatzikos 2002) that was modified for head image registration. First, the ICV in the template is manually and carefully delineated by an expert. Then, based on the HAMMER registration algorithm, the template with its ICV mask is warped to the space of each individual head. Finally, the warped ICV mask of the template is used to directly extract the ICV of the individual.

Statistical Analysis

The purpose of the statistical analysis is to assess the relationship between sulcal geometry and age. Within this study, we conduct both cross-sectional and longitudinal analyses in which we analyze measures including surface area, cortical thickness, GM volume, sulcal depth, local gyrification index, and mean curvature. The GM volume is used to assess cortical atrophy, and the other measures quantify cortical shape. The cross-sectional analysis involves individuals of different ages at the same time point, whereas the longitudinal analysis assesses age-related changes in the same individual over time.

We analyze 4 sulcal regions on each cortical hemisphere—the left and right central, left and right superior frontal, left and right cingulate, and left and right parietooccipital regions. We selected these regions primarily for 2 reasons. First, we determined that these regions could be robustly segmented and reliably labeled with our methods (Rettmann and others 2005). Second, we wanted to include regions on both the lateral and medial surfaces of the cortex. The central and superior

frontal sulci are located on the lateral surface, whereas the cingulate and parietooccipital sulci are located on the medial surface.

Before transferring the data sets from the BLSA database, the data set names were encoded such that the year of acquisition for each scan was unknown. Next, the cortical reconstructions and sulcal segmentations were generated for each data set. Upon visual inspection, the surface model generated for 1 data set appeared noisy and inaccurate and was therefore dropped from the analysis. The selected sulcal regions were manually identified on each of the 104 cortical surfaces using our sulcal-labeling interface (Rettmann and others 2005), and all labeling was performed by a single user (M.E.R.). Of the 832 sulcal regions labeled, 3 were not segmented correctly and were therefore dropped from the analysis.

Cross-sectional Analysis

The geometric features analyzed in the cross-sectional analysis were surface area, thickness, GM volume, mean geodesic depth, local gyrification index, percentage of high positive and negative curvature points, and percentage of very high negative curvature points. For each sulcal region, we computed the average of each of the geometric measurements across the 3 years. The partial correlation between age and each geometric measure was computed, adjusting for ICV to correct for individual differences in overall size. Using the false discovery rate (FDR) (Benjamini and Hochberg 1995) to control for multiple comparisons, only correlations with $P \leq 0.0015$ should be considered significant. Due to the exploratory nature of this work, however, we also present results with a trend toward significance. We consider results with a $0.0015 < P < 0.05$ to have a trend toward significance. All computations were done using SAS version 8.1 (SAS Institute, Cary, NC).

Longitudinal Analysis

The same geometric measures analyzed in the cross-sectional analysis were also analyzed in the longitudinal analysis. Analyses were conducted for each measure separately using repeated-measures multivariate analysis of variance, with time (year 1, year 3, and year 5) and hemisphere (right and left) as the repeated-measures factors. In this analysis, we do not adjust for ICV because our primary outcome measure is within-subject longitudinal change, which is not correlated with ICV for these measures. This was tested by first computing the difference between each measure at year 5 and year 1. Next, we computed correlation coefficients between these difference measures and ICV and found no significant correlations (using the FDR to control for multiple comparisons). In the longitudinal sulcal analysis, we again used the FDR to control for multiple comparisons and found that only correlations with $P \leq 0.0077$ should be considered significant. Due to the exploratory nature of this work, however, we also present results with a trend toward significance. We consider results with a $0.0077 < P < 0.05$ to have a trend toward significance.

Results

Cross-sectional

Correlations between age and geometric measurements are reported in Table 2 along with their associated *P* values. Only correlations with $P < 0.05$ are reported. The right and left central mean thicknesses are the only measures that reach significance using the FDR criterion; however, there are several other measurements with a trend toward significance. As indicated in the table, there is a negative correlation with age for both the left and right central sulcal regions with thickness and GM volume. The left and right cingulate sulcal regions have negative correlations with age for GM volume, mean geodesic depth, and high positive curvature. The right cingulate has a negative correlation with age for mean thickness and a positive correlation with age for percentage of high negative curvature points. The right superior frontal has a negative correlation with age for mean thickness, and the left parietooccipital has a negative correlation with age for percentage of very high negative curvature points.

Table 2
Correlations between age and measurements adjusted for ICV

Measure	Sulcal region	Correlation	*P* value
Mean thickness	Ce_l	−0.52	0.0015*
	Ce_r	−0.55	0.0007*
	SF_r	−0.41	0.0166
	$Cing_r$	−0.43	0.0110
Volume	Ce_l	−0.40	0.0189
	Ce_r	−0.41	0.0163
	$Cing_l$	−0.36	0.0388
	$Cing_r$	−0.40	0.0184
Mean depth	$Cing_l$	−0.40	0.0176
	$Cing_r$	−0.37	0.0312
Percentage of HP curvature	$Cing_l$	−0.47	0.0047
	$Cing_r$	−0.46	0.0067
Percentage of HN curvature	$Cing_r$	0.35	0.0411
Percentage of VHN curvature	PO_l	−0.35	0.0413

Note: Ce, central; SF, superior frontal; Cing, cingulate; PO, parietooccipital; l, left; r, right; HP, high positive; HN, high negative; VHN, very high negative. *Significant under FDR criterion.

Longitudinal

In this section, we report both significant results (indicated with an *) as well as results with trend toward significance. Several interesting time effects were observed in the longitudinal analysis. A longitudinal change in the area measurement was found for the parietooccipital sulcal region ($P = 0.0047$*; Fig. 8). Decreases in mean thickness were observed for the central ($P = 0.0215$) and cingulate ($P = 0.0413$) sulcal regions (Fig. 8). Decreases in GM volume were found in the central ($P = 0.0332$), superior frontal ($P = 0.0250$), and cingulate ($P < 0.0001$*) sulcal regions (Fig. 8). For the geodesic depth measure, we found a decrease in the mean depth of the parietooccipital sulcal region ($P = 0.0060$*; Fig. 8). The percentage of high positive curvature points decreased for the central ($P = 0.0077$*), cingulate ($P = 0.0192$), and parietooccipital ($P = 0.0006$*) sulcal regions (Fig. 9). The percentage of high negative curvature points increased for the cingulate ($P = 0.0336$) and parietooccipital ($P = 0.0114$) sulcal regions (Fig. 9). There were no significant time by hemisphere interactions, and there was only one with a trend toward significance, cingulate local gyrification index ($P = 0.0139$) where time has a greater effect on the left than the right.

Discussion

The aim of the current study was to determine whether age influences geometric properties of cortical morphology. We investigated a number of specific cortical regions using definitions based on sulcal regions. Despite the restricted age range of our older adult sample, our results reveal age effects on specific geometric properties in selected cortical regions. In this section, we summarize the results and discuss the general trends observed in the data.

The goal of the cross-sectional analysis was to determine if there are age differences in our sample of adults in the geometry of a set of sulcal regions. The correlations of mean thickness with age were negative, indicating that older individuals have thinner cortical GM. Other cross-sectional studies have also reported thinner cortices in older versus younger subjects (Magnotta and others 1999; Salat and others 2004). The most

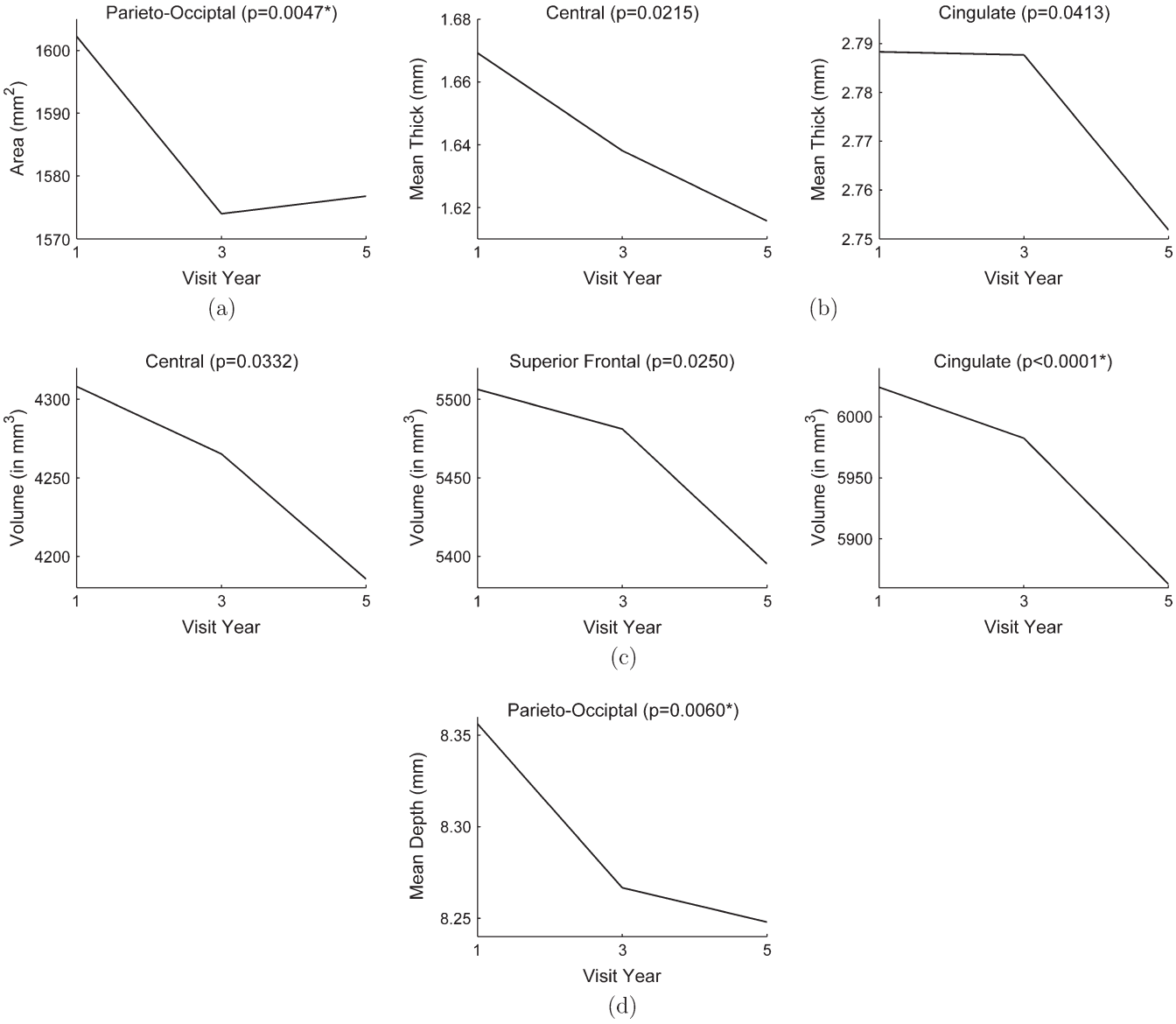

Figure 8. Plots have visit year on the *x* axis and (*a*) area, (*b*) mean thickness, (*c*) volume, and (*d*) mean depth averaged across all subjects on the *y* axis. *Significance under the FDR criterion.

consistent thickness finding occurred in the central sulcal region, which reached significance on both the right and the left side. This result is consistent with the findings in Salat and others (2004), where age differences in cortical thickness were prominent in the central sulcus. We also found negative correlations with age for the volume measurement, indicating smaller GM volumes in the central and cingulate sulcal regions for the older individuals. For the mean geodesic depth measurements, we found negative associations with age for both the left and the right cingulate sulcal regions, with older individuals having more shallow sulci than younger individuals. More shallow sulci could signify that older individuals have more "open" sulci than younger individuals—an indication of age-associated cortical shape differences.

We found negative associations with age for the percentage of high positive curvature points for both the left and right cingulate sulci with older individuals having a smaller percentage of high curvature points. The high positive curvature points correspond to highly convex points on the surface—that is, regions of the cortex bending "outward." A smaller percentage of these points in the cingulate sulcal region could be due to a variety of factors. One possibility is that the cingulate sulcus is more open, or wide, in the older individuals. This would make the gyral folds at the top of the sulcal region less sharp, resulting in lower positive curvature values. Another possible explanation is that older individuals have fewer outward bends within the sulcal region itself. On the other hand, when analyzing the percentage of high negative curvature points, we found a positive correlation with age in the right cingulate, indicating that older individuals have more inward bends than younger individuals in this region. In the analysis of very high negative curvature points, we found a negative correlation with age in the left parietooccipital sulcal region. Points of very high negative curvature correspond to the sharpest inward bends in the surface and mainly occur along the fundus, or bottom, of the sulcus. A smaller percentage of these points could signify

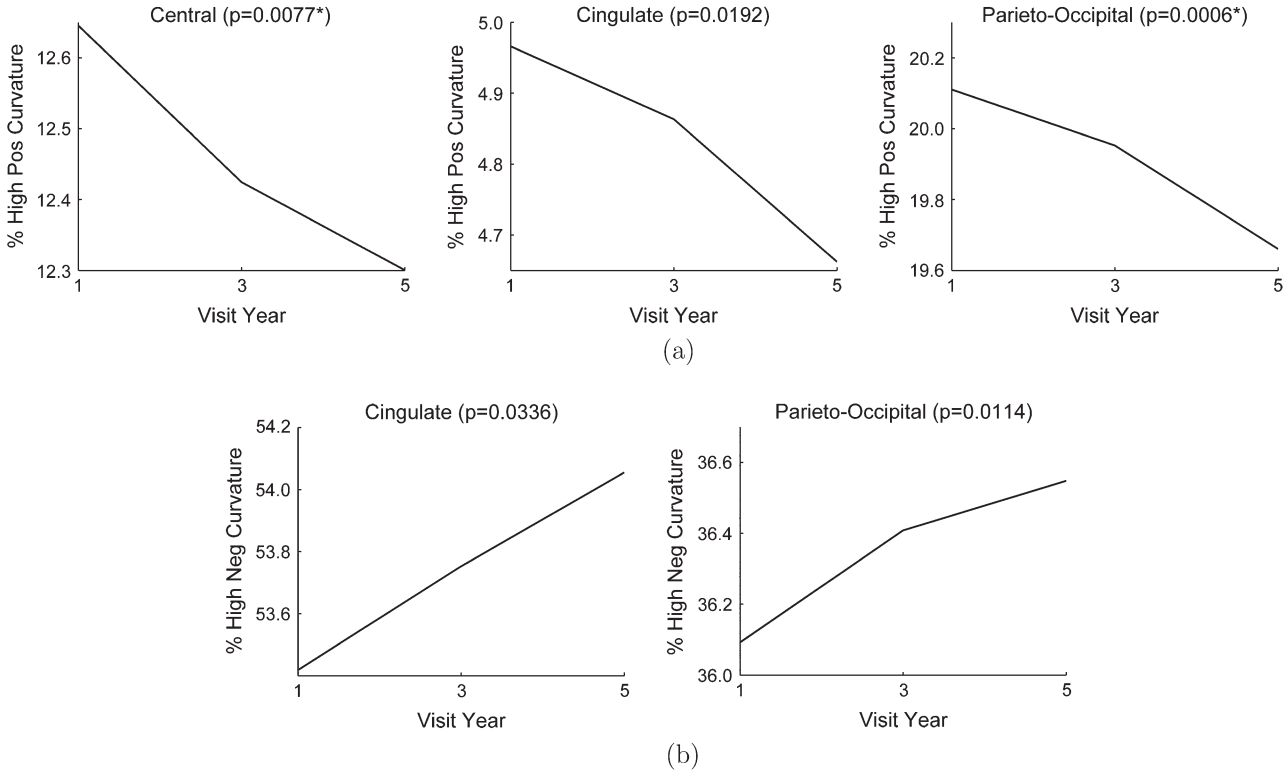

Figure 9. Plots have visit year on the *x* axis and (*a*) percentage of high positive curvature points and (*b*) percentage of high negative curvature points averaged across all subjects on the *y* axis. *Significance under the FDR criterion.

that the left parietooccipital sulcal fundus is less sharply folded in older versus younger individuals—another indication of a possible "opening up" of sulci with age. In general, we observed differences in older versus younger individuals in both the percentage of high positive and high negative curvature points in various sulcal regions.

The goal of the longitudinal analysis was to determine if sulcal geometry undergoes changes during aging. In this analysis, sulcal measurements for each individual were made three times over a 4-year time span. As this is a relatively short time period, we expected any measurable longitudinal changes to be small. In addition, because we have a fairly large age range of older adults in our sample, we expected to see similar changes in the measures from year 1 to year 3 and year 3 to year 5. This is true for a majority of the measures; however, some of the measures exhibit an apparent nonlinearity across visit years. This observation may represent greater measurement error in the 2-year interval than the 4-year interval.

In the analysis of mean thickness, we observed decreases in thickness for both the central and cingulate sulcal regions. This is consistent with the cross-sectional results where we found negative correlations in both the central and cingulate sulcal regions. We observed decreasing GM volumes in the central, superior frontal, and cingulate sulcal regions. GM loss in the cingulate sulcal region is consistent with the longitudinal findings in Resnick and others (2003) and the cross-sectional findings reported in Good and others (2001). Loss of GM in the central sulcal region is also consistent with the findings in Good and others (2001). For the geodesic depth measure, we observed a decrease in mean depth with time in the parieto-occipital sulcal region. We also found an overall decrease in surface area for this sulcal region over the 4-year time span; however, for this measure, we observed first a large decrease followed by a small increase. We suspect this small increase is due to measurement error.

For the positive mean curvature measure, we observed a decrease in the percentage of high positive curvature points in 3 of the 4 sulcal regions analyzed, indicating a "flattening out" of outward cortical bends with time. The decrease in cingulate high positive curvature points is consistent with the results from the cross-sectional analysis. On the other hand, we observed an increase in the percentage of high negative curvature points in 2 sulcal regions, indicating an increase in inward bending cortex with time. The increase in high negative curvature points in the cingulate sulcal region is consistent with the trend observed for the right cingulate in the cross-sectional results. These indications of changes in curvature with time merit further investigation to yield a more detailed understanding of the exact nature and location of these sulcal shape changes.

A wide variety of metrics was used in this study to characterize geometric cortical changes associated with aging. GM volume, thickness, and surface area are related in that they provide metrics of the amount of cortex contained within sulcal regions. GM volume, however, is the only metric that can truly characterize cortical atrophy. Although decreases in thickness may be an indicator of atrophy, there is the possibility that a decrease in thickness is instead due to a cortical shape change (i.e., stretching) and not due to true atrophy. In this case, thickness would decrease, surface area would increase, and volume would remain constant. In our sample, we primarily found concurrent decreases in GM volume and thickness (i.e., in

the central and cingulate regions), indicating that thinning is due to atrophy and not cortical stretching. Sulcal depth quantifies how far inward a sulcal fold extends into the cortex. A decrease in sulcal depth (i.e., the sulcus is becoming more shallow) could signify that the sulcus is opening up or becoming wider, which has been observed in other aging studies (Lancaster and others 2004). A decrease in sulcal depth is conceivably related to surface area because as a sulcal region becomes shallower, the surface area will also decrease. In our data set, we observed a concurrent longitudinal decline in the parietooccipital surface area and mean depth.

The curvature metrics, on the other hand, give a direct measure of cortical shape in terms of how the surface is bending. There may, however, be subtle relationships between curvature and other metrics. For example, if the decrease in high positive curvature points is due to the gyral folds at the top of the sulcal region becoming less sharp, there would be a concurrent decrease in sulcal depth because the distance to the gyral cortex will now be shorter. We observed this trend for the cingulate sulcal region in the cross-sectional analysis.

It is also possible there are relationships between changes in curvature and changes in thickness. For example, the flattening out of a sharp outward bend could be caused by cortical atrophy (which would result in a concurrent decline in thickness and GM volume) or cortical stretching (which would result in a concurrent decline in thickness but not GM volume). In this data set, we observed concurrent declines in high positive curvature points, GM volume, and thickness in the cingulate region both cross-sectionally and longitudinally. We also observed this concurrent decline longitudinally in the central sulcal region. This could be an indication that cortical flattening is related to cortical atrophy; however, a more detailed analysis of the localized regions undergoing curvature changes would be necessary to confirm this relationship.

Thus, the various metrics provide both complementary as well as related information. The metrics also differ in terms of statistical effect, sensitivity, convergence, and overall consistency. The largest number of significant results was observed with the thickness metric in the cross-sectional analysis and the percentage of high positive curvature points in the longitudinal analysis. The 2 most sensitive metrics are mean depth and percentage of high negative curvature points, detecting changes in the order of 1.2–1.3% in the longitudinal analysis. The mean geodesic depth was also found to be extremely reliable with a short-term test–retest repeatability of approximately 2% and an average long-term stability correlation of 0.95 (Rettmann 2003). Metrics with convergent bilateral results in the cross-sectional analysis were thickness, volume, depth, and percentage of high positive curvature points. Metrics that provide convergent results between the cross-sectional and longitudinal analyses were GM volume and thickness. Finally, if we define the most consistent findings to be those with both bilateral convergence cross-sectionally as well as convergent longitudinal results, we can conclude that the most consistent findings are decrease in central mean thickness, decrease in central GM volume, decrease in cingulate GM volume, and decrease in cingulate high positive curvature points.

In future work, we plan to use these techniques to analyze the entire BLSA data sets, which consists of 158 subjects scanned up to 11 years at present. To assist with analyzing these measures in a larger sample size, we are currently investigating automated methods for labeling the sulcal regions (Tosun and others 2004). In this larger sample size, we will also analyze sex differences in the context of morphological age changes. In addition, we will investigate whether these regional cortical measurements change differentially in normal, healthy aging as compared with aging accompanied by either cognitive impairment or Alzheimer's disease.

Notes

The authors thank Dzung Pham for assistance with the MR data. The authors also thank Dinggang Shen and Christos Davatzikos for computation of the ICVs. This work was supported in part by National Institute on Aging (NIA) by the Intramural Research Program of the National Institutes of Health, NIA.

Address correspondence to email: maryam.rettmann@nih.gov.

References

Ashburner J, Friston KJ. 2000. Voxel-based morphometry—the methods. Neuroimage 11(6 Pt 1):805–821.

Benjamini Y, Hochberg Y. 1995. Controlling the false discovery rate: a practical and powerful approach to multiple testing. J R Stat Soc Ser B 57(1):289–300.

Coffey CE, Wilkinson WE, Parashos IA, Soady SAR, Sullivan RJ, Patterson LJ, Figiel GS, Webb MC, Spritzer CE, Djang WT. 1992. Quantitative cerebral anatomy of the aging human brain: a cross-sectional study using magnetic resonance imaging. Neurology 42(3 Pt 1):527–536.

Courchesne E, Chisum HJ, Townsend J, Cowles A, Covington J, Egaas B, Harwood M, Hinds S, Press GA. 2000. Normal brain development and aging, quantitative analysis of in vivo MR imaging in healthy volunteers. Radiology 216(3):672–682.

Cowell P, Turetsky BI, Gur RC, Grossman RI, Shtasel DL, Gur RE. 1994. Sex differences in aging of the human frontal and temporal lobes. J Neurosci 14(8):4748–4755.

DeCarli C, Murphy DGM, Gillette JA, Haxby JV, Teichberg D, Schapiro MB, Horwitz B. 1994. Lack of age-related differences in temporal lobe volume of very healthy adults. Am J Neuroradiol 15(4):689–696.

Goldszal AF, Davatzikos C, Pham DL, Yan M, Bryan RN, Resnick SM. 1998. An image processing system for qualitative and quantitative volumetric analysis of brain images. J Comput Assisted Tomogr 22(5): 827–837.

Good CD, Johnsrude IS, Ashburner J, Henson RNA, Friston KJ, Frackowiak RSJ. 2001. A voxel-based morphometric study of ageing in 465 normal adult human brains. Neuroimage 14(1 Pt 1):21–36.

Gur RC, Mozley PD, Resnick SM, Gottlieb GL, Kohn M, Zimmerman R, Herman G, Atlas S, Grossman R, Berretta D, Erwin R, Gur RE. 1991. Gender differences in age effect on brain atrophy measured by magnetic resonance imaging. Proc Natl Acad Sci USA 88(7): 2845–2849.

Han X, Pham DL, Tosun D, Rettmann ME, Xu C, Prince JL. 2004. CRUISE: cortical reconstruction using implicit surface evolution. Neuroimage 23(3):997–1012.

Han X, Xu C, Braga-Neto U, Prince JL. 2002. Topology correction in brain cortex segmentation using a multiscale, graph-based algorithm. IEEE Trans Med Imaging 21:109–121.

Han X, Xu C, Prince JL. 2001. Cortical surface reconstruction using a topology preserving geometric deformable model. The Fifth IEEE Workshop on Mathematical Methods in Biomedical Image Analysis (MMBIA). Washington, DC: IEEE Computer Society. p 213–220.

Han X, Xu C, Prince JL. 2003. A topology preserving level set method for geometric deformable models. IEEE Trans Pattern Anal Mach Intell 25:755–768.

Han X, Xu C, Rettmann ME, Prince JL. 2001. Automatic segmentation editing for cortical surface reconstruction. Proceedings of International Society for Optical Engineering Medical Imaging, vol. 4322. Bellingham, WA: International Society for Optical Engineering. p 194–203.

Jernigan TL, Press GA, Hesselink JR. 1990. Methods for measuring brain morphologic features on magnetic resonance images. Validation and normal aging. Arch Neurol 47(1):27–32.

Kawas C, Gray S, Brookmeyer R, Fozard J, Zonderman A. 2000. Age-specific incidence rates of Alzheimer's disease: the Baltimore longitudinal study of aging. Neurology 54:2072–2077.

Kimmel R, Sethian JA. 1998. Computing geodesic paths on manifolds. Proc Natl Acad Sci USA 95:8431–8435.

Kochunov P, Mangin JF, Coyle T, Lancaster J, Thompson P, Riviere D, Cointepas Y, Regis J, Schlosser A, Royall DR, Zilles K, Mazziotta J, Toga A, Fox PT. 2005. Age-related morphology trends of cortical sulci. Hum Brain Mapp 26(3):210–220.

Lancaster J, Kochunov P, Mangin JF, Riviere D, Cointepas Y, Regis J, Fox PT. 2004. Age-related opening of cortical sulci. NeuroImage 22 (Suppl 1):S319.

Liu RSN, Lemieux L, Bell GS, Sisodiya SM, Shorvon SD, Sander JWAS, Duncan JS. 2003. A longitudinal study of brain morphometrics using quantitative magnetic resonance imaging and difference image analysis. Neuroimage 20(1):22–33.

Magnotta VA, Andreasen NC, Schultz SK, Harris G, Cizadlo T, Heckel D, Nopoulos P, Flaum M. 1999. Quantitative in vivo measurement of gyrification in the human brain: changes associated with aging. Cereb Cortex 9(2):151–160.

Mangin JF, Riviere D, Cachia A, Duchesnay E, Cointepas Y, Papadopoulos-Orfanos D, Collins DL, Evans AC, Regis J. 2004. Object-based morphometry of the cerebral cortex. IEEE Trans Med Imaging 23(8):968–982.

Meyer F, Beucher S. 1990. Morphological segmentation. J Vis Commun Image Representation 1(1):21–46.

Mueller EA, Moore MM, Kerr DCR, Sexton G, Camicioli RM, Howieson DB, Quinn JF, Kaye JA. 1998. Brain volume preserved in healthy elderly through the eleventh decade. Neurology 51(6):1555–1562.

Murphy DGM, DeCarli C, McIntosh AR, Daly E, Mentis MJ, Pietrini P, Szczepanik J, Schapiro MB, Grady CL, Horwitz B, Rapoport SI. 1996. Sex differences in human brain morphometry and metabolism: an in vivo quantitative magnetic resonance imaging and positron emission tomography study on the effect of aging. Arch Gen Psychiatry 53(7):585–594.

Ono M, Kubick S, Abernathey CD. 1990. Atlas of the cerebral sulci. New York: Thieme.

Pfefferbaum A, Mathalon DH, Sullivan EV, Rawles JM, Zipursky RB, Lim KO. 1994. A quantitative magnetic resonance imaging study of changes in brain morphology from infancy to late adulthood. Arch Neurol 51(9):874–887.

Pham DL. 2001. Spatial models for fuzzy clustering. Comput Vis Image Underst 84(2):285–297.

Pham DL, Prince JL. 1999. Adaptive fuzzy segmentation of magnetic resonance images. IEEE Trans Med Imaging 18(9):737–752.

Raz N, Gunning FM, Head D, Dupuis J̃H, McQuain J, Briggs SD, Loken WJ, Thornton AE, Acker JD. 1997. Selective aging of the human cerebral cortex observed in vivo: differential vulnerability of the prefrontal gray matter. Cereb Cortex 7(3):268–282.

Resnick SM, Goldszal AF, Davatzikos C, Golski S, Kraut MA, Metter EJ, Bryan RN, Zonderman AB. 2000. One-year age changes in MRI brain volumes in older adults. Cereb Cortex 10(5):464–472.

Resnick SM, Pham DL, Kraut MA, Zonderman AB, Davatzikos C. 2003. Longitudinal magnetic resonance imaging studies of older adults: a shrinking brain. J Neurosci 23(8):3295–3301.

Rettmann M. 2003. Analysis of regional cortical geometry using automated sulcal segmentation from a surface model of the human cerebral cortex [PhD thesis]. Baltimore, MD: Johns Hopkins University.

Rettmann ME, Han X, Xu C, Prince JL. 2002. Automated sulcal segmentation using watersheds on the cortical surface. Neuroimage 15(2):329–344.

Rettmann ME, Tosun D, Tao X, Resnick SM, Prince JL. 2005. Program for assisted labeling of sulcal regions (PALS): description and reliability. Neuroimage 24(2):398–416.

Salat DH, Buckner RL, Snyder AZ, Greve DN, Desikan RSR, Busa E, Morris JC, Dale AM, Fischl B. 2004. Thinning of the cerebral cortex in aging. Cereb Cortex 14(7):721–730.

Scahill RI, Frost C, Jenkins R, Whitwell JL, Rossor MN, Fox NC. 2003. A longitudinal study of brain volume changes in normal aging using serial registered magnetic resonance imaging. Arch Neurol 60(7):989–994.

Shen D, Davatzikos C. 2002. Hammer: hierarchical attribute matching mechanism for elastic registration. IEEE Trans Med Imaging 21(11):1421–1439.

Shock NW, Greulich RC, Andres R, Arenberg D, Costa PT Jr, Lakatta E, Tobin JD. 1984. Normal human aging: the Baltimore longitudinal study of aging. Washington, DC: US Government Printing Office.

Sowell ER, Peterson BS, Thompson PM, Welcome SE, Henkenius AL, Toga AW. 2003. Mapping cortical change across the human life span. Nat Neurosci 6(3):309–315.

Spitzer R, Williams J. 1987. Diagnostic and statistical manual of mental disorders DSM-III-R. 3rd ed rev. Washington, DC: American Psychiatric Association.

Sullivan EV, Marsh L, Mathalon DH, Lima KO, Pfefferbaum A. 1995. Age-related decline in MRI volumes of temporal lobe gray matter but not hippocampus. Neurobiol Aging 16(4):591–606.

Sullivan EV, Rosenbloom M, Serventi KL, Pfefferbaum A. 2004. Effects of age and sex on volumes of the thalamus, pons, and cortex. Neurobiol Aging 25(2):185–192.

Tang Y, Whitman GT, Lopez I, Baloh RW. 2001. Brain volume changes on longitudinal magnetic resonance imaging in normal older people. J Neuroimaging 11(4):393–400.

Tao X. 2005. Statistical geodesics and shape models: finding features for registering human cortical surfaces [PhD thesis]. Baltimore, MD: Johns Hopkins University.

Tisserand DJ, Pruessner JC, Sanz Arigita EJ, van Boxtel MPJ, Evans AC, Jolles J, Uylings HBM. 2002. Regional frontal cortical volumes decrease differentially in aging: an MRI study to compare volumetric approaches and voxel-based morphometry. Neuroimage 17(2):657–669.

Tosun D, Rettmann ME, Prince JL. 2004. Mapping techniques for aligning sulci across multiple brains. Med Image Anal 8(3):295–309.

Vincent L, Soille P. 1991. Watersheds in digital spaces: an efficient algorithm based on emersion simulations. IEEE Trans Pattern Anal Mach Intell 13(6):583–598.

Xu C, Han X, Prince JL. 2000. Improving cortical surface reconstruction accuracy using an anatomically consistent gray matter representation. NeuroImage 11(5 part 2):S581.

Xu C, Pham DL, Rettmann ME, Yu DN, Prince JL. 1999. Reconstruction of the human cerebral cortex from magnetic resonance images. IEEE Trans Med Imaging 18(6):467–480.

Zilles K, Armstrong E, Schleicher A, Kretschmann H. 1988. The human pattern of gyrification in the cerebral cortex. Anat Embryol 179(2):173–179.